ACS SENSORS

pubs.acs.org/acssensors

Article

Picomolar-Level Sensing of Cannabidiol by Metal Nanoparticles Functionalized with Chemically Induced Dimerization Binders

M. D. Ashif Ikbal,[#] Shoukai Kang,[#] Xiahui Chen, Liangcai Gu,[*] and Chao Wang[*]

Cite This: *ACS Sens.* 2023, 8, 4696−4706

Read Online

ACCESS | Metrics & More | Article Recommendations | Supporting Information

ABSTRACT: Simple and fast detection of small molecules is critical for health and environmental monitoring. Methods for chemical detection often use mass spectrometers or enzymes; the former relies on expensive equipment, and the latter is limited to those that can act as enzyme substrates. Affinity reagents like antibodies can target a variety of small-molecule analytes, but the detection requires the successful design of chemically conjugated targets or analogs for competitive binding assays. Here, we developed a generalizable method for the highly sensitive and specific in-solution detection of small molecules, using cannabidiol (CBD) as an example. Our sensing platform uses gold nanoparticles (AuNPs) functionalized with a pair of chemically induced dimerization (CID) nanobody binders (nanobinders), where CID triggers AuNP aggregation and sedimentation in the presence of CBD. Despite moderate binding affinities of the two nanobinders to CBD (equilibrium dissociation constants K_D of ∼6 and ∼56 μM), a scheme consisting of CBD−AuNP preanalytical incubation, centrifugation, and electronic detection (ICED) was devised to demonstrate a high sensitivity (limit of detection of ∼100 picomolar) in urine and saliva, a relatively short sensing time (∼2 h), a large dynamic range (5 logs), and a sufficiently high specificity to differentiate CBD from its analog, tetrahydrocannabinol. The high sensing performance was achieved with the multivalency of AuNP sensing, the ICED scheme that increases analyte concentrations in a small assay volume, and a portable electronic detector. This sensing system is readily applicable for wide molecular diagnostic applications.

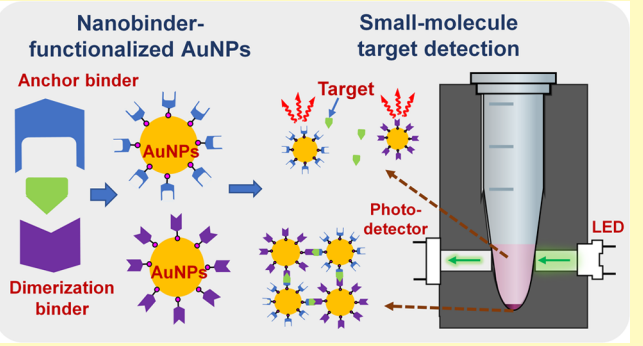

KEYWORDS: *small-molecule sensing, cannabidiol, chemically induced dimerization, metal nanoparticles, rapid electronic detection*

Small molecules are ubiquitous, taking the form of metabolites, drugs, toxins, etc.,[1−3] and have been explored for pain relief[4] and treatment of cardiac diseases,[5] cancers,[6] and infectious diseases[7] including COVID-19.[8] It is critical to differentiate relatively subtle differences in small molecules because they can encipher drastic differences in the molecular bioactivities. For example, delta-9-tetrahydrocannabinol (THC) and cannabidiol (CBD)[9,10] are two major constituents of cannabis with similar structures but different pharmacology and psychoactivity. The current gold-standard detection method is mass spectrometry,[11] which, however, is commonly used in centralized facilities instead of standardly equipped laboratories. Portable methods such as electrochemical glucose sensors[12] are highly useful, but the detection relies on the availability of a specific enzyme that recognizes the small-molecule substrate and thus is not widely applicable to any analyte. In comparison, affinity-based detection methods, such as an enzyme-linked immunosorbent assay (ELISA),[13,14] are complementary and more generalizable, but they typically require the labeling of small molecules for competitive binding assays, i.e., chemical conjugation of small-molecule targets or their competitive analog to solid support or reporter molecules.[15] In this regard, chemically induced dimerization (CID)[16,17] provides an ideal mechanism to directly sense small molecules via forming a ternary complex, making it suitable for in-solution detection without washing steps. Recently, we developed a method (COMBINES-CID) for creating CID systems by screening a combinatorial nanobody library applicable to different analytes.[18] CID binders for CBD were selected[18] and found to dimerize via a "molecular glue" mechanism.[19] Although an ELISA-like sandwich assay was applicable for CBD detection, such an assay required extensive sample incubation, washing, and spectrometric or fluorescent analysis, and thus, it was not suitable for portable detection. It is therefore necessary to develop a simple, fast sensing platform with a digital readout for a variety of analytes.

Here, we report a sensitive and rapid detecting system with an inexpensive optoelectronic readout that significantly

Received: August 24, 2023
Revised: November 3, 2023
Accepted: November 29, 2023
Published: December 12, 2023

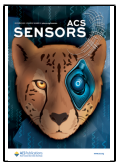

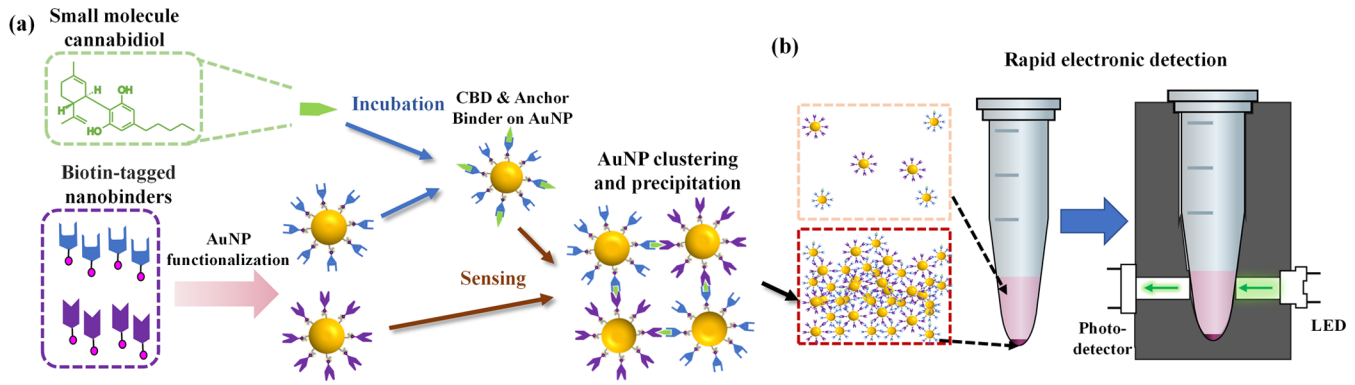

Figure 1. Overview of small-molecule detection. (a) Schematic showing key steps in enhanced CBD detection, including functionalization of AuNPs with nanobinders (anchor binder: blue; dimerization binder, purple), preincubation of CBD sample with anchor binder on AuNPs, and mixing the CBD-anchored AuNPs with dimerization-binder-functionalized AuNPs for reaction. (b) Schematics showing CBD molecule signal readout. Here, AuNP clusters form in the presence of CBD in the target sample. The LED serves as a light source to probe the floating AuNPs, and the photodetector converts the transmitted light into electronic signals.

improves the detection limit and reduces the detection time (from ∼5 to <2 h) compared to ELISA with the same CID nanobinder pair. Specifically, multivalent sensors were designed by conjugating synthetic nanobinders specific to the small molecules onto gold nanoparticles (AuNPs). Such nanobinders can dimerize with the small molecules, thus triggering aggregation and subsequent precipitation of AuNP sensors. This accordingly results in increased solution transparency correlated with small-molecule concentration. The modulation of solution color can be further quantified using a lab-based spectrometer or a portable optoelectronic readout system comprising simple and inexpensive components such as a light-emitting diode (LED), a photodiode, and a battery. Using CBD as the target, we demonstrate a new scheme consisting of CBD incubation with binder-functionalized AuNPs, centrifugation and electronic detection (ICED) to achieve a high sensitivity (<100 pM) in urine and saliva, a high specificity (distinguishing from CBD homologue THC), and a large dynamic range (5 logs). This ICED scheme strongly facilitates high-performance small-molecule recognition by the multivalent functionalization of binder pairs on AuNPs, localized detection of concentrated CBD via incubation on AuNPs and centrifugation, accelerated signal transduction from AuNP aggregation and precipitation, and low background noise from portable electronic detectors. This cost-effective (<$2 per test), portable, and accurate system can be advantageous in broad applications such as drug and toxin detection, biomarker diagnostics, drug discovery, etc.

CBD BINDER PROTEIN SELECTION

To obtain specific binders to the CBD molecules, a COMBINES-CID method was employed[18,20] to design the CBD CID system, isolated from a combinatorial nanobinder library of over 10^9 complementarity-determining region (CDR) peptide sequences. To obtain the CBD anchor binder (CA), six rounds of selection were performed using biotinylated CBD as bait, eventually obtaining three unique clones with high specificity. Using BioLayer interferometry (BLI) and isothermal calorimetry (ITC), we confirmed that the anchor binder alone can bind CBD with an affinity in the single-digit μM range.[18,19] CA14 (K_D = 6 μM), a binder with the highest protein yield, was then chosen as a bait for dimerization binder (DB) selection, producing 24 unique DBs after four rounds of biopanning. The two most stable CBD CID binder pairs identified by size-exclusion chromatography (SEC) and BLI, CA14−DB 21(K_D = 56 nM) and CA14−DB 18 (K_D = 560 nM), were expressed as a C-terminal Avi-tagged and His-tagged form in *Escherichia coli*, purified by Ni-affinity and biotinylated by BirA, and then site-specifically conjugated to AuNPs as previously reported.[21] The specific sequences of CA14, DB18, and DB 21 can be found in Table S1.

PREPARATION OF MULTIVALENT SMALL-MOLECULE SENSOR

To prepare for the CBD small-molecule assay, we examined AuNPs covalently coated with high-density streptavidin proteins (e.g., estimated ∼1300 binding sites for 80 nm AuNPs) for sensing, conceptually similar to our recently reported antigen sensors.[21] Upon mixing with biotinylated nanobinders (anchor binder CA14 and dimerization binders DB18 or DB21), these AuNPs formed multivalent sensors (Figure 1a). Upon the introduction of small molecules, these multivalent in-solution sensors display improved effective affinity, beneficial for accelerated molecular binding and higher sensitivity compared to monovalent detection systems.[22,23] The molecular recognition is accompanied by aggregation of the AuNP sensors, resulting in sedimentation. This sedimentation-based detection mechanism differs fundamentally from other plasmonic colorimetric assays, where the detection is based on resonance wavelength shift caused by the formation of dimers and oligomers of small AuNPs (5−20 nm) still present in the solution.[24−26] Here, the use of larger AuNPs produces nanosensors of bigger surface areas, which accordingly hosts more nanobinders and presents a high binding affinity for high-quality multivalent molecular recognition. Further, larger NP sizes also make them more responsive to centrifugation-enhanced target molecule binding and NP precipitation (Figure 1b), which is important to shortening the assay time limit (e.g., demonstrated 2 h, compared to 5 h by incubation only) and improving the detection. In addition, our precipitation-enhanced, molecule-concentration-dependent modulation of AuNP clustering allows accurate signal readout by probing the optical extinction of free-floating AuNPs. Therefore, the molecular signals can be converted to electronic output by fundamentally a pair of simple LEDs and photodetectors operating at the AuNP extinction wavelengths

https://doi.org/10.1021/acssensors.3c01758
ACS Sens. 2023, 8, 4696−4706

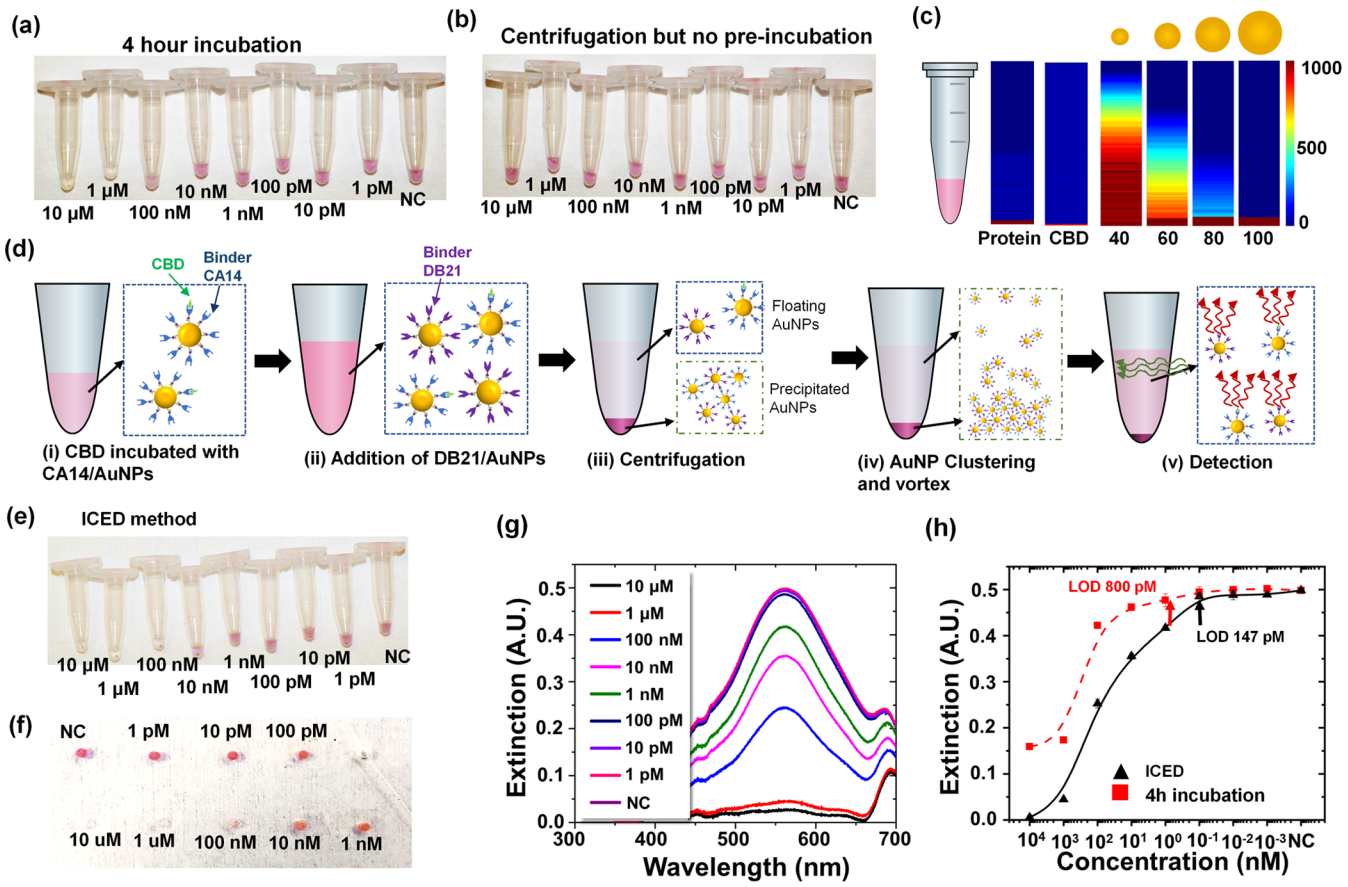

Figure 2. ICED detection of CBD molecule in PBS buffer. (a, b) Optical images of microcentrifuge tubes of CBD detection: (a) CBD mixed with CA14- and DB 21-functionalized AuNPs, and then 4 h incubation was applied (protocol in Figure S1). (b) CBD mixed with functionalized AuNPs, then centrifuged, incubated for 20 min, and vortexed (protocol in Figure S3). (c) Calculated molecule and AuNP distributions across liquid height after centrifugation. (d) Schematic showing the process flow of ICED detection of CBD molecule. Here, CA14-functionalized AuNPs were preincubated with to-be-tested CBD samples prior to mixing with DB 21-functionalized AuNPs for sensing (protocol in Figure S5). (e, f) Optical images of CBD detection using the ICED method: (e) microcentrifuge tubes; (f) PDMS plate image of the extracted top liquid from panel (e). (g) Extinction spectra of AuNPs from PDMS plate in panel (f). (h) Extinction peak values (at 559 nm) for ICED method (extracted from plot (g), black triangle) and after 4 h of incubation (red squares).

(Figure 1c), enabling portable, rapid, accurate, inexpensive, and digital diagnostics. This method is fundamentally different from and much simpler than conventional optical sensing methods that analyze the complete spectra using bulky and expensive microscopy and spectrometers.

PREANALYTICAL INCUBATION AND CENTRIFUGATION-ENHANCED DETECTION

As discovered in our previous work,[21] the sample preparation methods, particularly incubation and centrifugation, have a significant impact on the sensing accuracy and detection time of the AuNP sensors. Here, we have compared two methods for CBD detection, i.e., incubation only (schematic and results in Figures S1 and S2) and a new approach termed ICED, namely, preanalytical Incubation of CBD with binder-functionalized AuNPs, Centrifugation, and Electronic Detection. For the incubation-only approach, 80 nm of AuNPs coated with purified CA14 and DB 21 was incubated with the CBD molecules for 4 h (Figure 2a). Then, the top 5 μL liquid was pipet-loaded in a custom-made PDMS plate reader and spectroscopically measured using a UV−visible spectrometer coupled to an upright microscope. A significant color contrast was observed between 100 nM CBD and the negative control (NC, i.e., blank sample with only buffer) (Figure 2a). To quantify the CBD detection, we further extracted the extinction intensity at the peak wavelength (~560 nm) for 80 nm of AuNPs and plotted it against CBD concentrations. The incubation-based sensing yielded a limit of detection (LOD) of ~0.7 nM (Figure 2h), comparable to the sandwich ELISA-based detection method applied previously with the same set of cobinding CID system (LOD of ~0.8 nM for ELISA).[15] The incubation-based system proved the feasibility of detecting small molecules such as CBD with a detection time similar to ELISA (typically around 5 h) but still much faster than traditional mass-spec systems.

To further improve the assay sensitivity and reduce the assay time, we theoretically studied the impact of the AuNP sedimentation process on sensing. In such a AuNP-based sensing system, two critical parameters governing the assay time and performance are aggregation time constant τ_a and sedimentation time constant τ_s. In determining τ_a, we employed a simplified version of Smoluchowski's coagulation equation[27] to estimate an empirical parameter P, defined as the probability of a binding event resulting from each molecular collision, and found that the best estimated P value was ~1. This indicated that the multivalence of the conjugated AuNPs increased the potential binding affinity compared to the monobinding process,[22,23] significantly different from tradi-

https://doi.org/10.1021/acssensors.3c01758
ACS Sens. 2023, 8, 4696−4706

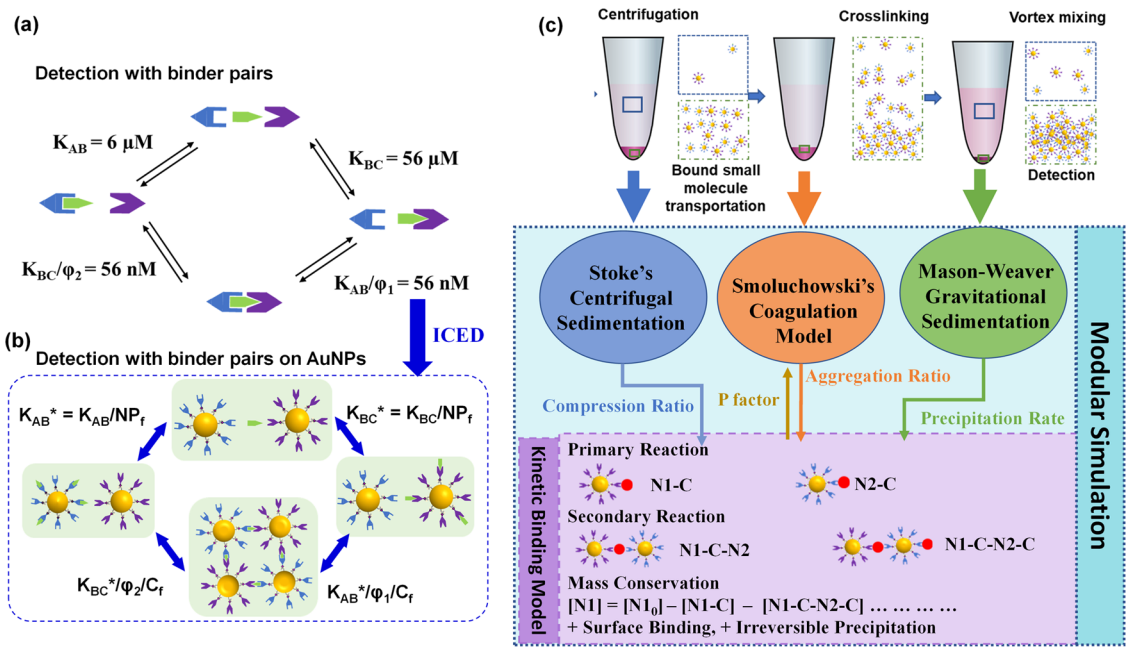

Figure 3. Modular analytic model for the ICED assay. (a, b) Schematics showing the enhancement in effective binding affinity with AuNPs: (a) a typical sandwich assay with an effective binding affinity of 56 nM using a pair of anchor binder (CBD binding affinity of 6 μM) and dimerization binder (CBD binding affinity of 56 μM); (b) the use of multivalent AuNPs effectively improves the binding affinity by a factor of C_f. (c) Model framework showing modular simulation strategy comprising individual physical models used to simulate reaction mechanism for multivalent AuNP aggregation and sedimentation-based biosensing system.

tional surface-based detection such as ELISA.[28,29] This also implied that ELISA-determined binding constants were nonideal to precisely predict the effective affinity observed in our solution-based multivalent sensing system. Additionally, τ_a can also be reduced significantly by increasing the AuNP concentration, which could be achieved by applying centrifugation to localize the AuNPs at the tube bottom. Further, we calculated $\tau_s = z/(s \cdot g)$ using the Mason−Weaver equation,[30,31] where z is the precipitation path (e.g., the height of the colloid liquid), g is the gravitation constant, and s is the sedimentation coefficient dependent on the physical properties of AuNPs and buffers.[30] This suggested that larger AuNP clusters, formed during CBD to nanobinder binding, would precipitate rather quickly. Assisted by simulation, we could also visualize that 80 nm AuNPs had a very narrow equilibrium gradient distribution in micromolar concentration,[30,31] more specifically that most of the dimers and trimers resided at the tube bottom. Given that the signals were collected from only the top-layer solution, only floating monomers modulated the observed optical extinction intensity, while the precipitated AuNP dimers or oligomers would not contribute to the solution signals.

The theoretical analysis pointed out that increasing the AuNP concentration and decreasing the liquid height, i.e., volume, would enable us to detect CBD faster. However, too high of a AuNP concentration would have resulted in the saturation of optical extinction at a lower CBD concentration, thus lowering detectability. On the other hand, it is challenging to reliably collect the signals only from free-floating AuNPs in the top liquid of a very small liquid volume. We applied a centrifugation approach to accelerate the detection (schematic in Figure S3), similar to the method we employed in rapid Ebola and SARS-CoV-2 antigen sensing.[21] However, the incubation time (1−20 min) used for protein sensing was found insufficient here to produce a visible color change except at the highest (10 μM) CBD concentration (Figure 2b). To investigate this phenomenon, we used the Stokes centrifugal force equation to calculate the spatial distribution of particles (Figures 2c and S4) under centrifugal force[32] for CBD, proteins, and AuNPs of different sizes from 40 to 100 nm. The simulation showed that this centrifugation step, although effectively concentrating the AuNPs at the bottom of the tube within about 2 min, is incapable of concentrating CBD. Still broadly distributed within the tubes, the amount of CBD molecules at the tube bottom was rather limited, and therefore the CBD-induced AuNP clustering process was slow and could be mainly CBD diffusion-limited.

To circumvent this slow reaction issue, in our new ICED approach, we developed a strategy to enhance CBD concentration for improved detection. To do so, we opted to use the higher affinity binder CA14 from the CA14−DB 21 pair (6 μM for CA14 compared to 56 μM for DB 21) as a CBD carrier to transport target CBD molecules to the reaction zone at the tube bottom. More specifically, we preincubated the CA14-coated AuNPs with CBD for 2 h, followed by mixing with the DB 21-coated AuNPs and centrifugation (Figure 2d and more data in Figures S5 and S6). The sample tubes were incubated for 20 min to form stable AuNP clusters from the CBD reaction to CA and DB binders and then briefly vortexed to release the monomer AuNPs that did not participate in the CBD reaction to retain a high selectivity in detection. This nanobinder/AuNP-mediated preincubation of CBD (Figure 2e) evidently improved the detection of CBD (Figure 2e). The concentration-dependent CBD sensing results were further quantified by extracting the top 5 μL in a PDMS plate (Figure 2f), examining their optical extinction (Figure 2g), and recording the extinction peaking values at the AuNP resonance (560 nm) (Figure 2h). Clearly, the incubation-based (red line, Figure 2h) and ICED methods (black line, Figure 2h) displayed similar concentration-dependent signal modulation;

https://doi.org/10.1021/acssensors.3c01758
ACS Sens. 2023, 8, 4696−4706

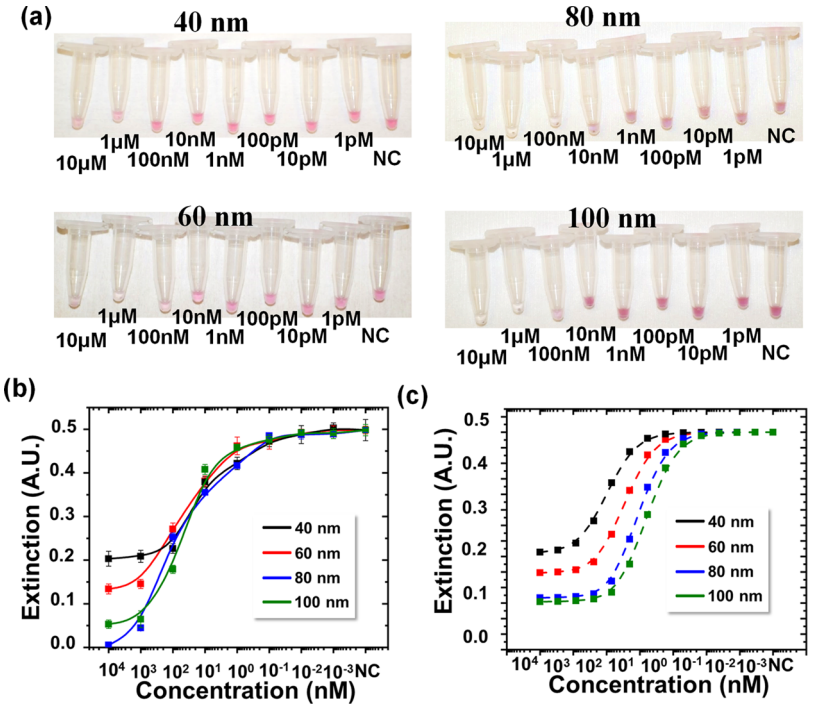

Figure 4. Experimental and simulation analyses of the nanoparticle size effect on CBD detection. (a) Optical images of CBD detection in PBS for AuNP sizes of 40, 60, 80, and 100 nm. The pictures were taken after all reactions. Initial and intermediate-stage images are provided in Supporting Figures. (b) Extracted optical extinction peak values for CBD detection in PBS for different nanoparticle sizes. (c) Simulated extinction peak values for CBD detection for dimerization system CA14−CBD−DB 21.

however, the LOD for the ICED method (~144 pM) was about 5 times better than the incubation-based detection (~700 pM) and the traditional sandwich ELISA with the same reagents (~800 pM).[11]

MODULAR ANALYTIC MODEL FOR SENSOR OPTIMIZATION

The underlying detection mechanism involves multidisciplinary studies of complex biochemical binding between the target molecule to binder pairs and physical processes for AuNP clustering and sedimentation, and therefore, a number of factors, including multivalent molecular binding, sedimentation time, aggregation, etc., can affect the assay preformation. In order to better verify the working mechanism, we tested CBD with AuNPs, extracted the top-level liquid, and diluted for nanoparticle tracking analysis (NTA) measurement (Supporting Figure S7a). From the NC sample, the AuNP size distribution (average 80 nm, 3-sigma deviation 20 nm) was consistent with expectation, considering the coating of streptavidin and nanobinders on the AuNPs. Such NTA analysis served to verify that the top liquid contained only monomers of the functionalized AuNPs. In addition, we also extracted 2 μL of liquid of all of the samples from the tube bottom, dried the liquid, and imaged the samples by transmission electron microscopy (TEM) (Supporting Figures S7b and S8). Clearly, only AuNP monomers were observed for the NC sample, evidently showing minimal nonspecific AuNP clustering, but AuNP clusters of different sizes were only found for CBD concentrations from 100 pM to 1 μM. The TEM imaging analysis proved the AuNP cluster formation and growth with the molecule concentration, which is important to understanding the signal transduction mechanism from molecule binding to optical and electronic detection. However, the cluster size analysis from TEM is constrained by its high cost, unavoidable human errors in sample preparation, and imaging limitations in measuring the cluster depth that obscure accurate determination of the amount of AuNPs within the cluster. On the other hand, we believe that the sizes of the formed clusters depend not only on the target molecule concentrations but also other factors, such as the binding affinity of nanobinders to the target molecule, incubation time, centrifugation speed/time, and vortex speed/time. Future studies to combine a comprehensive experimental analysis of various factors with fluidic dynamic simulations would help to better elucidate the complex process.

In this work, in order to formulate a model to better understand the complex chemical reactions and fluidic dynamics involving CBD molecules, nanobinders, and AuNPs, we created a modular analytic model (Figure 3). Briefly, we started with a dynamic model for the reaction kinetics in combination with Smoluchowski's coagulation equation and utilized two different coagulation models, i.e., Mason−Weaver equation for gravitational sedimentation and Stokes' equation for centrifugal sedimentation, to parameterize the initial conditions as well as to predict the aggregate precipitation. Additionally, we identified two parametric factors that correlate to the enhancement effect of our system, i.e., NPf signifies the multivalence effect of the nanoparticle sensor (proportional to the surface area or d^2), while Cf signifies the nanoparticle concentration effect by centrifugation. In addition, preincubation was introduced to favor the chemical reaction of capture nanobinder (CA14) and CBD to form the AuNP−CA14−CBD complexes (Figure 3a). We found that NPf = 50 and Cf = 100 produced the best experimental fitting for our assay using 80 nm of AuNPs (Figure S9a). The chemical reactions during the ICED sensing process strongly

https://doi.org/10.1021/acssensors.3c01758
ACS Sens. 2023, 8, 4696−4706

depend on the concentrations of the CBD, which directly affect the amount of the formed AuNP−CA14−CBD complex, and the centrifugation process, which modulates the local concentration of the AuNP-based complexes. Taking into account the centrifugation effect in simulation (Figure S9b), it is clear that the incubation-based assay (red curve, Cf = 0) had a much worse signal contrast in optical extinction at the highest analyte concentrations (10 μM) compared to that with the ICED approach (black curve, Cf = 100). In principle, the aggregation of AuNP−CA14−CBD−DB (21/18)−AuNP into AuNP oligomers or clusters could happen immediately after mixing the AuNP−CA14−CBD and AuNP−DB (21/18) solutions. However, given the affinity of CBD binders, the formation of large AuNP clusters is thought to require an extensive long reaction time, particularly at low CBD concentrations. Therefore, the formation of AuNP clusters, which is critical to reliable signal transduction, would be a very slow process without centrifugation. In contrast, the centrifugation process, although not expected to significantly modulate the concentrations of free-floating CBD molecules, can effectively spin down the AuNPs and therefore greatly enhance the local concentrations of AuNP−CA14−CBD complexes and also DB (21/18)−AuNP complexes. As a result, the AuNP cluster formation rate can significantly increase during centrifugation and incubation period.

Further, we also simulated the impact of the inherent antigen−antibody binding affinity on the assay performance (Figure S9c), where two different nanobinder systems CA14−DB 21 (K_D = 56 nM) and CA14-DB18 (K_D = 560 nM) were used. Interestingly, despite that DB18 has 1 order of magnitude lower binding affinity, its predicted sensing signal contrast, i.e., the optical extinction intensity difference at the highest CBD concentration (10 μM) from the NC signal, was only moderately worse (at 0.18) compared to that from DB 21 (0.08). This is partially attributed to the fact that DB18 has a higher K_D (560 nM compared to 56 nM) but a comparable association constant (k_{on}).[10] The molecular dissociation is partly compensated for by the use of multivalent in-solution AuNPs coated with many binders, which effectively promotes stronger binding. Further, the precipitation-based readout was much less reversible and more favorable compared with monolayer analyte binding in a conventional ELISA assay. Lastly, a good agreement between our model fitting for the 80 nm AuNP and the experimental results proved the validity of our analytical model to guide sensor design and optimization in similar affinity-based assays, from the sensing of small molecules to proteins and even to nucleic acids. In addition, coupling modeling with experimental analysis will also serve to better design and screen the performance of the designed synthetic nanobinders.

■ ASSAY OPTIMIZATION: IMPACT OF NANOPARTICLE SIZES ON SENSING

To evaluate the role nanoparticle size plays in CBD detection, we employed the CBD ICED assay with different AuNP sizes (40, 60, 80, and 100 nm) (Figure 4a−d and more data in Supporting Figures S10−S13). Clearly, the color of the 1 μM CBD concentration could be easily differentiated from the NC sample for all AuNP sizes. However, further analysis of the extinction signals shows that 80 and 100 nm AuNPs were better in dynamic range and LOD (Figure 4b). Additionally, the impact of AuNP size was also evaluated by our modeling (Figure 4c). Clearly, the signal intensity contrast was much higher for larger nanoparticles (0.5 for 80 nm AuNPs and 0.45 for 100 nm AuNPs) than for smaller ones (0.3 for 40 nm AuNPs and 0.35 for 60 nm AuNPs, respectively). This can be attributed to two factors, i.e., effective sedimentation described previously (Section 2.3) and effective concentration $[NP]_e$. Here, $[NP]_e$ of a multivalent nanoparticle sensor is defined as the product of the concentration of the nanoparticle [NP] and the amount of surface ligands per NP [S] following $[NP]_e \propto [NP][S]$.

Fundamentally, our sensor essentially monitors the localized surface plasmon resonance (LSPR) extinction of free-floating AuNPs. The LSPR extinction is dependent on the AuNP concentration [NP] and diameter d roughly following $\sigma_{ext} \propto [NP]d^3$[29], and therefore the AuNP concentration in our test was lower at larger sizes following $[NP] \propto \frac{1}{d^3}$, considering equal extinctions of AuNPs for different sizes in our experiments. Further considering that [S] is also related to the surface area and hence diameter of the particles as $[S] \propto d^2$, we obtain $[NP]_e \propto 1/d$. Therefore, a higher $[NP]_e$ for relatively small AuNPs under our experimental conditions was favored to promote reaction and signal readout. Indeed, too large nanoparticles (>100 nm) from the manufacturer (Cytodiagnosics) did not perform well due to their much lower particle concentrations available from the manufacturer and much broader extinction spectra.

However, on the other hand, the sedimentation time also increases with smaller AuNPs. This is particularly true for detection by only incubation, where typically a few hours are needed for effective AuNP clustering and subsequent precipitation. In comparison, for the ICED method, the use of centrifugation effectively concentrates the AuNPs to promote faster reaction. For example, we have performed Stokes' centrifugal simulation (Figure S4) to show that a 2 min centrifugation at 1200g could concentrate 80 nm of AuNPs by a factor of ∼50 but only by ∼10 for 40 nm AuNPs. Clearly, smaller nanoparticles still occupy a larger volume than 80 nm of AuNPs after centrifugation. This results in a longer precipitation path and a longer sedimentation time, diminishing their advantage in a higher particle concentration. In general, we observed a good overall agreement on the effect of nanoparticle size (Figure 4b,c) between experiments and model prediction. Experimentally, 80 nm of AuNPs performed better than 100 nm of AuNPs and, thus, was chosen as the primary design for CBD sensing.

■ NANOBINDER IMPACT

Further, two nanobinder pairs CA14/DB 21 (K_D = 56 nM when sandwiching CBD) and CA14/DB18 (K_D = 560 nM for CBD) were compared for their sensing performance. Even though the overall binding affinity of DB 21 was 10 times higher compared to that using DB18, its resulting LOD was only 5 times better than that of DB18 (Figures 5a, S5, S6, and S14). This could be attributed to a high k_{on} value of DB18, which is comparable to that of DB 21, and the induced AuNP aggregation. As predicted in our model (Figure S9c) and verified by our experiments, we suspect that binders with comparable binding affinity but with high k_{on} and dissociation (k_{off}) constants would be beneficial to produce a better LOD because high dissociation would be partially suppressed by the presence of multivalent binding sites on the AuNPs, which essentially suppresses dissociation and promotes AuNP clustering. Clearly, this example suggests the complexity of

https://doi.org/10.1021/acssensors.3c01758
ACS Sens. 2023, 8, 4696−4706

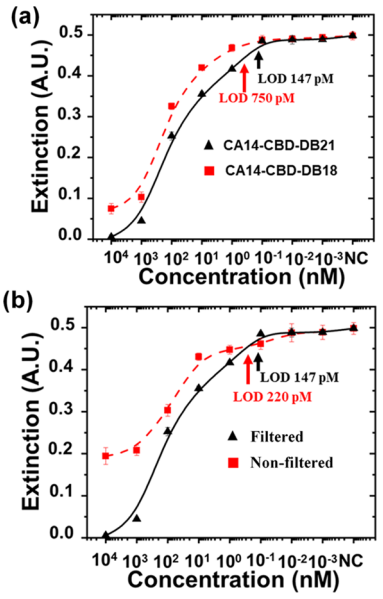

Figure 5. Impact of nanobinder and reagent filtration on CBD detection. (a) Extracted optical extinction peak for CBD detection in PBS for dimerization systems CA14−CBD−DB 21 (black triangle with a solid line) and CA14−CBD−DB 21 (red square with a dashed line). (b) Extracted optical extinction peak values for CBD detection in PBS for the standard ICED approach (sensors filtered, black triangle with a solid line) and simplified ICED approach (not filtrated, red square with a dashed line) assay.

the sensing system and the importance of a combination of analytic modeling and experimentation in studying the reaction mechanism. Further, it may also shed light on the designs and selection of antibodies and nanobinders, where both the binding affinity and the association constants may play important roles.

SIMPLIFIED SENSOR PREPARATION WITHOUT FILTRATION

The coupled experimental and modeling analysis proved that our design strategy was successful in small-molecule analyte detection in body fluids with greatly improved sensitivity compared to ELISA. To further explore the feasibility with an even simpler sensor preparation scheme, we tested our system using nanoparticle sensors with a simplified process by eliminating the purification step, which worked to remove excessive reagents after mixing the nanobinder solutions with AuNPs. In particular, 80 nm of streptavidin-coated AuNPs was mixed with biotinylated nanobinders at a molar ratio of 1:400 and incubated for 30 min and then used to detect CBD following the ICED method. The simplified approach had slightly worse performance (LOD of 220 pM) compared to the standard approach using filtered AuNPs (LOD ∼ 147 pM, Figure 5b, and additional data in Figures S15−S19), possibly due to the presence of partially conjugated AuNPs and excessive unbound nanobinders (Figure S20). However, this approach eliminated the purification process and also reduced the consumption of AuNPs and nanobinder solutions (Table 1), therefore saving both cost and time. This sample preparation method could be particularly of interest in applications in which cost and accessibility are of great importance.

DETECTION OF CBD IN URINE AND SALIVA USING A PORTABLE ELECTRONIC DETECTION SYSTEM

To further facilitate portable CBD detection, we demonstrated a portable electronic detection (PED) system comprising a tandem LED and a photodiode system (Figure 6a). The LED emits at a wavelength matching that of the 80 nm AuNP extinction peak, and the light passing through the upper-level liquid was collected by a photodiode, where electrical signals were produced and adjusted using a serially connected load resistor. For demonstration, a snug-fit microcentrifuge holder was 3D-printed, where windows were open to define the optical path along the upper portion of the liquid. The PED system was validated to produce a large dynamic range so that large variations in CBD concentration could be measured without saturation. In practice, we measured CBD in 5% urine and saliva, in both testing tubes (Figures 6b,c, S21, and S22) and PDMS well plate. The optical measurement results showed an LOD of ∼165 and ∼198 pM for CBD spiked in urine and saliva (Figure 6d,e and Table S2), as well as a broad dynamic range (5 logs) and excellent specificity against THC (Figure 6d,e and additional data in Figures S23 and S24). In comparison, the PED system further improved the LOD to ∼88.5 and ∼97.5 pM for urine and saliva, respectively, or ∼8 times better than tested by ELISA.[18] As an example, the typical concentrations of CBD and THC in oral fluids for cannabis smokers reach as high as ∼100 and >1000 μg/L after drug

Table 1. Summary of Key Experimental Design Parameters as well as Reagent Use and Time Consumption in Different Detection Schemes Tested in This Work

key parameters	parameter details	incubation only	centrifuge without preincubation	ICED with filtration	ICED without filtration
nanosensor preparation-related	AuNP to nanobinder molar ratio	1:2560	1:2560	1:2560	1:400
	filtration to remove excessive binders	yes	yes	yes	no
sensing protocol related	premixing incubation	no	no	2 h	2 h
	centrifugation	no	yes	yes	yes
	postmixing incubation	NA	20 min	20 min	20 min
time	sensing only	4 h	20 min	2 h and 20 min	2 h and 20 min
	total (including sensor preparation)	7−8 h	4−5 h	5−6 h	3−4 h
AuNP consumption	volume per test	16 μL	16 μL	16 μL	∼10 μL
	cost per test	∼$1.6	∼$1.6	∼$1.6	∼$1
nanobinder consumption	volume (at ∼1.5 μM)	3.6 μL	3.6 μL	3.6 μL	0.3 μL
	amount	5.3 pmol	5.3 pmol	5.3 pmol	0.5 pmol
LOD	optically measured in PBS buffer	790 pM	NA	147 pM	220 pM

https://doi.org/10.1021/acssensors.3c01758
ACS Sens. 2023, 8, 4696−4706

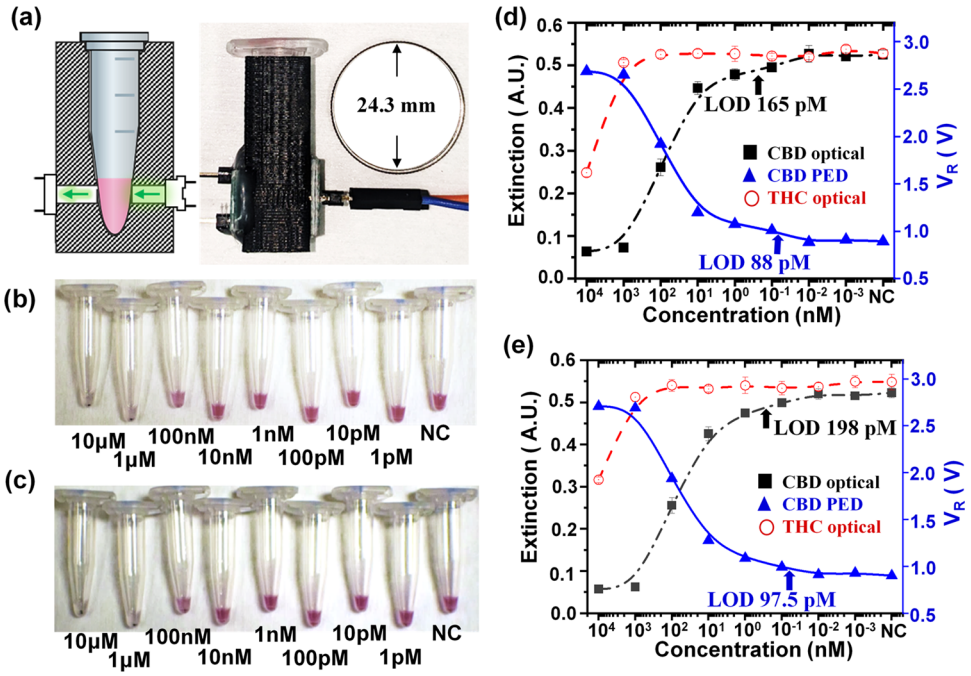

Figure 6. Rapid and portable electronic detection of CBD molecule in urine and saliva. (a) Schematic and optical image of the PED system, consisting mainly of an LED circuit, a photodiode circuit, and a 3D-printed tube holder. A coin with its size marked is pictured as a reference. (b) Optical image of detecting CBD spiked in urine. (c) Optical image of detecting CBD spiked in saliva. (d,e) CBD and THC sensing in (d) urine and (e) saliva. The CBD-containing urine and saliva solutions are 20% prior to mixing with AuNP sensors but 5% in the final mixture. Optical extinction peak values (559 nm) in CBD sensing (black squares and fitted dash-dot line) and THC sensing (red open-circle and dash line) were extracted from their optical spectra (Figures S21e and S22e for CBD and Figures S23e and S24e for THC). The electronic voltage signals of CBD (blue triangles and solid line) are directly measured from the tube samples shown in panels (b, c).

administration but drops to ~0.1 μg/L 5−24 h after.[33] The acceptable cutoff diagnostic concentrations for CBD and THC are 0.2−2 ng/mL but set as ~1 ng/mL by the European Driving Under the Influence of Drugs, Alcohol, and Medicines (DRUID). The CBD sensitivity on our platform (~100 pM or 0.03 μg/L) clearly proves its feasibility to detect small-molecule targets from clinically relevant samples. In addition, the ~4 log higher LOD in THC detection (1.24 μM in urine and 1.9 μM in saliva) indicates that the two closely relevant molecules can be easily differentiated on our sensing platform, proving highly specific detection. This PED-enhanced performance can be attributed to lower 3-σ errors generated during electronic measurements.[21] With a small footprint, low-cost readout device (a few dollars), low reagent cost (estimated < $2 for each test),[21] reliable yet simple operation, and a potential for automatic data collection, the PED-based small-molecule detection method has great potential for affordable diagnostic applications.

CONCLUSIONS

We have demonstrated a generalized rapid assay design to achieve sensitive detection of small molecules, using CBD (MW 314.47 g/mol), an important molecular target in the detection of drug misuse,[34] as an example. Here, a multileveled sensitivity-enhancing scheme has been innovated. First, a pair of nanobinder was used to form a stable sandwich with CBD at an improved affinity (56 nM compared to 6 and 56 μM individually). Second, multivalent AuNP sensors were used, each hosting hundreds of binding sites, thus greatly improving the effective binding affinity. In addition, we introduced a new ICED (i.e., brief incubation followed by centrifugation prior to electronic detection) to attach CBD to one set of AuNP sensors. The centrifugation process transports CBD molecules to the reaction zones at the testing tube bottom, thus greatly localizing the CBD and boosting their concentration prior to detection for improved sensitivity while decreasing the detection time. In addition, the AuNP aggregation and sedimentation occur in the presence of targeted small molecules, enabling CBD-concentration-dependent optical extinction display and subsequent portable electronic readout, which does not collect signals from other background materials and minimizes the background noise. As a result, this new sensing method can overcome the traditional challenges of forming reliable readout signals from low-affinity small-molecule binders, instead achieving high sensitivity (<100 pM), large dynamic range (5 logs), and high specificity against THC in biological medium. Additionally, this assay format eliminates long incubation or cumbersome washing steps typically required for ELISA or surface-based detection and greatly decreased the footprint for readout, making it an ideal platform for affordable and accessible detection in resource-limited regions.

MATERIALS AND METHODS

Materials. Phosphate-buffered saline (PBS) was purchased from Fisher Scientific. Bovine serum albumin (BSA) and molecular biology grade glycerol were purchased from Sigma-Aldrich. Sylgard-184 silicone elastomer kit was purchased from Dow Chemical. DNase/RNase-free distilled water used in the experiments was purchased from Fisher Scientific. The streptavidin-functionalized AuNPs were purchased from Cytodiagnostics, dispersed in 20% v/v glycerol and 1 wt % BSA buffer.

Nanobinder Generation, Selection, Expression, and Biotinylation. Nanobinders were generated using a previously established method.[18,19] In brief, rationally designed CDR sequences

https://doi.org/10.1021/acssensors.3c01758
ACS Sens. 2023, 8, 4696−4706

of different ratios of amino acids were used to generate a library of nanobinders. To obtain CBD anchor binders (CA), the library was screened using biotinylated CBD as a bait. The CBD-bound phage was eluted by unlabeled CBD. After six rounds of selection, three unique clones were identified by single phage ELISA. To select the CBD-induced dimerization binders, we chose CA14 as the anchor binder. Four rounds of biopanning were carried out using both CBD-free and CBD-bound CA14. Out of 384 clones screened, 24 unique clones were recognized using ELISA. All nanobinders were C-terminal Avi-tagged before biotinylation. Nanobinders bearing AviTag were biotinylated by BirA using a BirA-500 kit (Avidity).

Preparation of Nanobinder Surface-Functionalized AuNP Colloidal Solution. AuNPs of different sizes can be used for experimentation and optimization; here, the methodologies are provided using 80 nm of AuNPs. Streptavidin-functionalized 80 nm gold nanoparticles at a 0.13 nM concentration were mixed with biotinylated nanobinders (capture binder and different dimerization binders) in excess and incubated for 2 h to ensure complete streptavidin−biotin conjugation. Next, centrifuge purification (accuSpin Micro 17, Thermo Fisher) was applied at 10,000 rounds per minute (rpm, or ∼9650 *g*) for 10 min, and the top supernatant was discarded. This procedure was repeated twice to ensure a high-quality purification. The concentration of purified 80 nm AuNP colloidal solution was measured by a Nanodrop 2000 (Thermo Fisher) and readjusted to 0.048 nM. In our design, the optical extinction of the mixed detection solution for negative control should have a normalized value (in reference to the extinction of blank buffer solution) within 0.5 and 0.7 in order to enable a large dynamic range from picomolar to micromolar and a high sensitivity for CBD detection. Excessive AuNPs at low analyte concentration could lead to very low optical transmission to reach the photodetectors, thus challenging sensitive detection. Insufficient AuNPs, on the other hand, could be completely consumed to form precipitates at moderate CBD concentrations, thus limiting the maximum detectable concentration and dynamic range. The buffer used for mixing, dilution, purification, and subsequent readjustment contained 1× PBS with 20 vol % of glycerol and 1 wt % of BSA, prepared from 10× PBS powder, ultrapure water, glycerol, and BSA. This buffer was used to ensure AuNP sensor stability and minimize nonspecific interactions.

Preparation of CBD and THC Analyte Solution. CBD and THC solutions were serially diluted from 10 μM to 1 pM in detection media, which typically contained 1× PBS with 20 vol % of glycerol and 1 wt % of BSA. For detection in urine and saliva, this buffer was readjusted to have 1× PBS with 20 vol % of glycerol, 1 wt % of BSA, and 20 vol % of either urine or saliva. Upon mixing with AuNP sensor solutions, the final concentrations of CBD, THC, urine, and saliva in the sensing mixture are diluted 4 times (e.g., 5% for urine and saliva).

ICED Detection. CBD of different concentrations was preincubated for 2 h with the capture antibody-functionalized AuNP (CA14−AuNP) colloidal solution at a 2:3 volume ratio or 6 and 9 μL, respectively. This was done to ensure maximum surface coverage with the CBD−CA14−AuNP complex. Then, the chosen dimerization-binder-functionalized AuNP (DB 21/DB18-AuNP) was mixed with the preincubated colloidal solution at a volume ratio of CBD: CA14−AuNP: DB (21 or 18)-AuNP at 2:3:3, or 6, 9, and 9 μL, respectively. For electronic sensing in the microcentrifuge tube, the total solution volume was designed to be around 24 μL, given the microcentrifuge geometry and the LED mount position on the tube chamber. The design allows the LED emission to pass through the supernatant of the solution after reaction and best probe the free-floating AuNPs for optimal signal transduction. After mixing, the solution was centrifuged at 3500 rpm (∼1200 *g*) for 1 min. After incubation at a chosen time (typically 20 min), this colloidal solution was vortexed at 2100 rpm for 5 s to resuspend the monomers from the precipitates. The vortex agitation served to retain the selectivity to differentiate CBD molecules of different concentrations from negative controls.

TEM Sample Preparation and Imaging. To image AuNP precipitates, the supernatant was removed from the tube and 2−3 μL of AuNP sample colloid containing AuNP precipitates was left in the tube. The tube was then vortexed thoroughly. Samples of 2 μL were pipetted and coated on both sides of the oxygen plasma-treated Cu grid (Electron Microscopy Sciences, C flat, hole size 1.2 μm, hole spacing 1.3 μm). Then, 30 s of oxygen plasma was used for cleaning.

PDMS Well Plate Fabrication. PDMS well plate was created from Sylgard-184 elastomer. As detailed in our previous work, the PDMS was cured in a plain Petri dish with a thickness of 2.5 mm. The PDMS film was cut into the desired size, and 2 mm diameter holes were drilled with biopsy punch. Subsequently, it was treated with oxygen plasma and bonded to a glass slide of desired size.

Spectrometric Measurement. The UV−visible spectra and dark-field imaging were performed using a customized optical system (Horiba), comprising an upright fluorescence microscope (Olympus BX53), a broad-band 75 W xenon lamp (PowerArc), an imaging spectrometer system (Horiba iHR320, spectral resolution of 0.15 nm), a low-noise CCD spectrometer (Horiba Syncerity), a vision camera, a variety of filter cubes, operation software, and a high-power computer. Light transmitted through the PDMS well plate was collected by a 50 × objective lens (NA = 0.8). The focal plane was chosen at the well plate surface to display the best contrast at the hole edge.

Electronic Measurement. An LED−photodiode PED system was designed with three key components: an LED light source, a photodiode, and a microcentrifuge tube holder. The centrifuge tube holder was 3D-printed using an ABSplus P430 thermoplastic. An 8.6 mm diameter recess was designed to snuggly fit a standard 0.5 mL Eppendorf tube. Holes of 2.8 mm diameter were open on two sides of the microcentrifuge tube holder to align an LED (597−3311−407NF, Dialight), the upper-level assay liquid, and a photodiode (SFH 2270R, Osram Opto Semiconductors). The LED was powered by two Duracell optimum AA batteries (3 V) through a serially connected 35 Ω resistor to set the LED operating point. The photodiode was reversely biased by three Duracell optimum AA batteries (4.5 V) and serially connected to a 7 MΩ load resistor. The photocurrent that responds to the intensity of light transmitted through the assay was converted to voltage through the 7 MΩ load resistor and measured with a portable multimeter (AstroAI AM33D).

Signal Analysis and LOD Calculation. For optical detection in a given medium (buffer, saliva, and urine) from the PDMS well plate, a background signal calibration was performed. For each sample, 5 measurements were collected and averaged to obtain the test signal E_{test} (C) for each CBD concentration C. The background extinction E_{ref} from a blank sample filled with buffer is used as a reference. Therefore, the CBD signal was normalized as $S(C) = \frac{E_{ref} - E_{test}(c)}{E_{ref}}$. To calculate the standard deviation of the measurement methods (σ), we compared three different methods for estimation. The first method uses the signal variations of blank (or NC) sample (σ_{NC}), the second method measures the signal variations from a few lowest concentrations (pooled sigma from 4 lowest concentrations here, or σ_{PS4}), and the third method analyzes the variation from all measured concentrations (pooled sigma for all, or σ_{PSA}). The limit of detection (LOD) is therefore determined from S(LoD) = S(NC) − 3σ or graphically visualized (Figure S25) as the intercept on the sensing curves offset by 3σ from the NC signals. It was noticed that the σ_{NC} approach negatively affected the consistency in LOD determination (Table S2), possibly attributed to the inherent errors in optical focusing from one measurement to another. In comparison, σ_{PS4} and σ_{PSA} are better estimates, and σ_{PSA} provides better consistency in LOD estimation, minimizing the impact of errors from the NC measurement. For consistency, in this work, we chose σ_{PSA} to report the LOD values. In electronic measurements, a similar analytical principle was applied but the measured voltage signals were directly plotted.

Cost Analysis. The cost per test can be estimated by the amount of AuNPs, binders, and testing accessories. Here, considering reagent loss during purification (assuming ∼60% loss in the calculation), 16 μL of streptavidin-coated AuNPs (Cytodiagnostics, estimated ∼$0.1/μL at 0.13 nM concentration) is required to produce sufficient AuNP sensors for one test (Table 1). Therefore, the cost of AuNPs is ∼$1.6 per test. The cost for biotinylated nanobinder selection, purification, and production is estimated at ∼$4000/g. The amount of

https://doi.org/10.1021/acssensors.3c01758
ACS Sens. 2023, 8, 4696−4706

nanobinders (~15 kDa) needed to functionalize the AuNPs is 0.13 nM × 16 μL × 2560 = 5.3 pmol (or ~80 ng, i.e., $0.0032). Considering tubes (assuming $0.05) and buffer (≪$0.01), the total reagent cost is estimated at $1.7 per test. Using the simplified sensor preparation approach, the reagent loss can be further minimized, requiring ~10 μL of AuNP (~$1 per test) and only 0.5 pmol of nanobinders. The cost of large-scale-produced sensors could be much less and estimated < $0.01 per test previously.[21]

■ ASSOCIATED CONTENT

Supporting Information

Preprint of this manuscript is available on bioRxiv.[35] The Supporting Information is available free of charge at https://pubs.acs.org/doi/10.1021/acssensors.3c01758.

Supporting schemes, figures, and experimental data on (1) AuNP-based CBD detection, (2) the impact of nanoparticle size on CBD sensing, (3) the impact of nanobinders and sensor purification on CBD sensing, (4) CBD and THC sensing in urine and saliva, (5) table summarizing sensing performance under different experimental protocols, and (6) table listing the sequences of anchor and dimerization binders (PDF)

■ AUTHOR INFORMATION

Corresponding Authors

Liangcai Gu − *Department of Biochemistry, University of Washington, Seattle, Washington 98195, United States; Center of Excellence in Neurobiology of Addiction, Pain, and Emotion, Seattle, Washington 98195, United States;* orcid.org/0000-0002-8232-6025; Email: gulc@uw.edu

Chao Wang − *School of Electrical, Computer and Energy Engineering, Arizona State University, Tempe, Arizona 85287, United States; Biodesign Center for Molecular Design and Biomimetics and Centre for Photonic Innovation, Arizona State University, Tempe, Arizona 85287, United States;* orcid.org/0000-0001-5020-961X; Email: wangch@asu.edu

Authors

M. D. Ashif Ikbal − *School of Electrical, Computer and Energy Engineering, Arizona State University, Tempe, Arizona 85287, United States; Biodesign Center for Molecular Design and Biomimetics and Centre for Photonic Innovation, Arizona State University, Tempe, Arizona 85287, United States*

Shoukai Kang − *Department of Biochemistry, University of Washington, Seattle, Washington 98195, United States; Center of Excellence in Neurobiology of Addiction, Pain, and Emotion, Seattle, Washington 98195, United States*

Xiahui Chen − *School of Electrical, Computer and Energy Engineering, Arizona State University, Tempe, Arizona 85287, United States; Biodesign Center for Molecular Design and Biomimetics and Centre for Photonic Innovation, Arizona State University, Tempe, Arizona 85287, United States*

Complete contact information is available at: https://pubs.acs.org/10.1021/acssensors.3c01758

Author Contributions

#M.D.A.I. and S.K. contributed equally to this work. L.G. and S.K. designed, selected, and purified the nanobinders. M.A.I., X.C., and C.W. designed the readout systems, established the sensing protocols, performed the sensing experiments and characterization, and analyzed the data. The manuscript was written by M.A.I. and C.W. through important contributions of all authors. All authors have given approval to the final version of the manuscript.

Notes

The authors declare no competing financial interest.

■ ACKNOWLEDGMENTS

This work was supported by grants from the U.S. National Institutes of Health (NIH) (1R35GM128918, R21DA051555, and R21DA051194) to L.G. C.W. and M.A.I. acknowledge partial support from National Science Foundation (NSF) under grant nos. 1847324 and 2020464 and NIH under grant no. R21AI169098. The samples were characterized by the Eyring Materials Center (EMC) at Arizona State University. Access to EMC was supported, in part, by NSF grant no. 1542160.

■ REFERENCES

(1) Ruscito, A.; DeRosa, M. C. Small-molecule binding aptamers: Selection strategies, characterization, and applications. *Front. Chem.* **2016**, *4*, No. 14, DOI: 10.3389/fchem.2016.00014.

(2) Puscasu, A.; Zanchetta, M.; Posocco, B.; Bunka, D.; Tartaggia, S.; Toffoli, G. Development and validation of a selective SPR aptasensor for the detection of anticancer drug irinotecan in human plasma samples. *Anal. Bioanal. Chem.* **2021**, *413*, 1225−1236.

(3) Tartaggia, S.; Meneghello, A.; Bellotto, O.; Poetto, A. S.; Zanchetta, M.; Posocco, B.; Bunka, D.; Polo, F.; Toffoli, G. An SPR investigation into the therapeutic drug monitoring of the anticancer drug imatinib with selective aptamers operating in human plasma. *Analyst* **2021**, *146*, 1714−1724.

(4) Armenian, P.; Vo, K. T.; Barr-Walker, J.; Lynch, K. L. Fentanyl, fentanyl analogs and novel synthetic opioids: a comprehensive review. *Neuropharmacology* **2018**, *134*, 121−132.

(5) McKinsey, T. A.; Kass, D. A. Small-molecule therapies for cardiac hypertrophy: moving beneath the cell surface. *Nat. Rev. Drug Discovery* **2007**, *6*, 617−635.

(6) Zhang, J.; Yang, P. L.; Gray, N. S. Targeting cancer with small molecule kinase inhibitors. *Nat. Rev. Cancer* **2009**, *9*, 28−39.

(7) Santoro, M. G.; Carafoli, E. Remdesivir: from Ebola to COVID-19. *Biochem. Biophys. Res. Commun.* **2021**, *538*, 145−150.

(8) Lo, M. K.; Albariño, C. G.; Perry, J. K.; Chang, S.; Tchesnokov, E. P.; Guerrero, L.; Chakrabarti, A.; Shrivastava-Ranjan, P.; Chatterjee, P.; McMullan, L. K. Remdesivir targets a structurally analogous region of the Ebola virus and SARS-CoV-2 polymerases. *Proc. Natl. Acad. Sci. U.S.A.* **2020**, *117*, 26946−26954, DOI: 10.1073/pnas.2012294117.

(9) Devinsky, O.; Cilio, M. R.; Cross, H.; Fernandez-Ruiz, J.; French, J.; Hill, C.; Katz, R.; Di Marzo, V.; Jutras-Aswad, D.; Notcutt, W. G. Cannabidiol: pharmacology and potential therapeutic role in epilepsy and other neuropsychiatric disorders. *Epilepsia* **2014**, *55*, 791−802, DOI: 10.1111/epi.12631.

(10) Potter, D. J.; Clark, P.; Brown, M. B. Potency of Δ9−THC and other cannabinoids in cannabis in England in 2005: Implications for psychoactivity and pharmacology. *J. Forensic Sci.* **2008**, *53*, 90−94.

(11) Fu, L.; Zhang, J.; Si, T. Recent advances in high-throughput mass spectrometry that accelerates enzyme engineering for biofuel research. *BMC Energy* **2020**, *2*, No. 1, DOI: 10.1186/s42500-020-0011-8.

(12) Wang, J. Electrochemical glucose biosensors. *Chem. Rev.* **2008**, *108*, 814−825.

(13) Li, D.; Ying, Y.; Wu, J.; Niessner, R.; Knopp, D. Comparison of monomeric and polymeric horseradish peroxidase as labels in competitive ELISA for small molecule detection. *Microchim. Acta* **2013**, *180*, 711−717.

(14) Smolinska-Kempisty, K.; Guerreiro, A.; Canfarotta, F.; Cáceres, C.; Whitcombe, M. J.; Piletsky, S. A comparison of the performance of

molecularly imprinted polymer nanoparticles for small molecule targets and antibodies in the ELISA format. *Sci. Rep.* **2016**, *6*, No. 37638, DOI: 10.1038/srep37638.
(15) Li, Y.; Zhang, G.; Mao, X.; Yang, S.; De Ruyck, K.; Wu, Y. High sensitivity immunoassays for small molecule compounds detection—Novel noncompetitive immunoassay designs. *TrAC, Trends Anal. Chem.* **2018**, *103*, 198−208.
(16) Spencer, D. M.; Wandless, T. J.; Schreiber, S. L.; Crabtree, G. R. Controlling signal transduction with synthetic ligands. *Science* **1993**, *262*, 1019.
(17) Stanton, B. Z.; Chory, E. J.; Crabtree, G. R. Chemically induced proximity in biology and medicine. *Science* **2018**, *359*, No. eaao5902, DOI: 10.1126/science.aao5902.
(18) Kang, S.; Davidsen, K.; Gomez-Castillo, L.; Jiang, H.; Fu, X.; Li, Z.; Liang, Y.; Jahn, M.; Moussa, M.; DiMaio, F. COMBINES-CID: An efficient method for de novo engineering of highly specific chemically induced protein dimerization systems. *J. Am. Chem. Soc.* **2019**, *141*, 10948−10952, DOI: 10.1021/jacs.9b03522.
(19) Cao, S.; Kang, S.; Mao, H.; Yao, J.; Gu, L.; Zheng, N. Defining molecular glues with a dual-nanobody cannabidiol sensor. *Nat. Commun.* **2022**, *13*, No. 815, DOI: 10.1038/s41467-022-28507-1.
(20) Gomez-Castillo, L.; Watanabe, K.; Jiang, H.; Kang, S.; Gu, L. Creating highly specific chemically induced protein dimerization systems by stepwise phage selection of a combinatorial single-domain antibody library. *J. Visualized Exp.* **2020**, *155*, No. e60738, DOI: 10.3791/60738.
(21) Chen, X.; Kang, S.; Ikbal, A.; Zhao, Z.; Pan, Y.; Zuo, J.; Gu, L.; Wang, C. Synthetic nanobody-functionalized nanoparticles for accelerated development of rapid, accessible detection of viral antigens. *Biosens. Bioelectron.* **2022**, *202*, No. 113971, DOI: 10.1016/j.bios.2022.113971.
(22) Greenspan, N. S.; Cooper, L. J. Cooperative Binding by Mouse IgG3 Antibodies: Implications for Functional Affinity, Effector Function, and Isotype Restriction. In *Springer Seminars in Immunopathology*; Springer, 1993; pp 275−291.
(23) Hornick, C. L.; Karush, F. Antibody affinity—III the role of multivalence. *Immunochemistry* **1972**, *9*, 325−340.
(24) Alsager, O. A.; Kumar, S.; Willmott, G. R.; McNatty, K. P.; Hodgkiss, J. M. Small molecule detection in solution via the size contraction response of aptamer functionalized nanoparticles. *Biosens. Bioelectron.* **2014**, *57*, 262−268.
(25) Kim, T.; Lee, C.-H.; Joo, S.-W.; Lee, K. Kinetics of gold nanoparticle aggregation: experiments and modeling. *J. Colloid Interface Sci.* **2008**, *318*, 238−243.
(26) Kim, A.-R.; Kim, S.-H.; Kim, D.; Cho, S. W.; Son, A.; Yoon, M.-Y. Detection of nonylphenol with a gold-nanoparticle-based small-molecule sensing system using an ssDNA aptamer. *Int. J. Mol. Sci.* **2020**, *21*, 208.
(27) Deaconu, M.; Tanré, E.*Smoluchowski's Coagulation Equation: Probabilistic Interpretation of Solutions for Constant, Additive and Multiplicative Kernels*; Annali della Scuola Normale Superioredi Pisa, Classe di Scienze, 2000; Vol. *29*, pp 549−579.
(28) Piehler, J.; Schreiber, G. Biophysical analysis of the interaction of human ifnar2 expressed in E. coli with IFNα2. *J. Mol. Biol.* **1999**, *289*, 57−67.
(29) Rich, R. L.; Cannon, M. J.; Jenkins, J.; Pandian, P.; Sundaram, S.; Magyar, R.; Brockman, J.; Lambert, J.; Myszka, D. G. Extracting kinetic rate constants from surface plasmon resonance array systems. *Anal. Biochem.* **2008**, *373*, 112−120.
(30) Midelet, J.; El-Sagheer, A. H.; Brown, T.; Kanaras, A. G.; Werts, M. H. The sedimentation of colloidal nanoparticles in solution and its study using quantitative digital photography. *Part. Part. Syst. Charact.* **2017**, *34*, No. 1700095, DOI: 10.1002/ppsc.201700095.
(31) Abbott, S. Gravitational Sedimentation Calculator. https://www.stevenabbott.co.uk/practical-solubility/Gravitational-Sedimentation.php (accessed 2021).
(32) Bonaccorso, F.; Zerbetto, M.; Ferrari, A. C.; Amendola, V. Sorting Nanoparticles by Centrifugal Fields in Clean Media. *J. Phys. Chem. C* **2013**, *117*, 13217−13229.
(33) Swortwood, M. J.; Newmeyer, M. N.; Andersson, M.; Abulseoud, O. A.; Scheidweiler, K. B.; Huestis, M. A. Cannabinoid disposition in oral fluid after controlled smoked, vaporized, and oral cannabis administration. *Drug Test. Anal.* **2017**, *9*, 905−915.
(34) Hen-Shoval, D.; Amar, S.; Shbiro, L.; Smoum, R.; Haj, C. G.; Mechoulam, R.; Zalsman, G.; Weller, A.; Shoval, G. Acute oral cannabidiolic acid methyl ester reduces depression-like behavior in two genetic animal models of depression. *Behav. Brain Res.* **2018**, *351*, 1−3.
(35) Ikbal, M. A.; Kang, S.; Chen, X.; Gu, L.; Wang, C. Picomolar-Level Sensing of Cannabidiol by Metal Nanoparticles Functionalized with Chemically Induced Dimerization Binders, Submission date September 17, 2023, accessed on November 27, 2023, *bioRxiv* DOI: 10.1101/2023.09.13.557660.